Phycoerythrin- and cychrome-conjugated monoclonal antibodies specific for CD4 and CD8 were from PharMingen. Single-cell suspensions were prepared from thymus and lymph node. Ten thousand live cells were collected for each sample.

Enzyme-linked immunosorbent assay (ELISA)

We measured serum immunoglobulin levels by ELISA (Southern Biotechnology Associates). Plates were coated with goat anti-mouse immunoglobulin-μ, -γ and -α and developed with horseradish peroxidase-conjugated goat antibodies specific for each mouse immunoglobulin isotype. The concentrations were calculated using the linear ranges of the dilution and purified mouse immunoglobulin isotypes as standards.

Cell preparation and culture

Dendritic cells were generated as described[20]. Briefly, cells were flushed from the bone marrow cavity with PBS/2.5% FCS. Cells were plated at 1×10^6 cells per well in 2 ml DMEM, 25 mM HEPES and 10% FCS without phenol red, and 10 ng ml^{-1} GM-CSF and 1 ng ml^{-1} IL-4. Cells were cultured on 25-mm circular coverslips, with changes of medium every second day; non-adherent cells were removed by gentle washing. For activation, LPS (5 μg ml^{-1}) was added for the last 20 h of culture.

Epidermal sheet preparation

Ear snips were obtained from MHC II-EGFP mice, and hairs were removed using an epilating agent (Nair, Carter Products). Epidermal sheets were generated by separation of ear snips into dorsal and ventral halves, with the use of forceps.

Imaging of MHC II-EGFP molecules in dendritic cells

We used 5-day-old bone marrow dendritic cells for real-time imaging. For dissection of early and late endocytic compartments, dendritic cells were incubated with 25 μg ml^{-1} transferrin Alexa Fluor 594 (Molecular Probes) or DiI-LDL (10 μg ml^{-1}; provided by M. Krieger) for 30 min at 37 °C in DMEM without serum and washed three times. Similarly, dendritic cells were incubated with DsRed1-labelled (Clontech) *S. typhimurium* (provided by M. Starnbach) in normal medium without penicillin/streptomycin for 1 h, and analysed after a total of 3–5 h. Images were captured with an inverted Zeiss 200M microscope equipped with a ×63 objective (1.4NA PanApo) and a spinning-wheel confocal head (Perkin-Elmer), and supplied with a 37 °C open perfusion temperature-controlled chamber (20/20 Technology). We used Slidebook (Intelligent Imaging Innovation Inc) for image acquisition and data processing. Volocity (Improvision Inc) was used for creating a three-dimensional rendition of the volume.

Antigen presentation in real time

Dendritic cells at a concentration of 1×10^6 per coverslip were incubated with 300 μM HEL or Ova (Sigma) to induce display of antigen-derived peptides on class II molecules. Dendritic cells were then washed three times with culture medium. T cells (0.5×10^6) were labelled with the nuclear dye Hoechst 33258 (Molecular Probes), washed and then added to each coverslip containing dendritic cells. The HEL-specific T-cell hybridoma used was H46.13, which is specific for HEL(46–61) (provided by C. Alfonso); the Ova-specific T-cell hybridoma was B097.1, which is specific for Ova(323–339) (provided by P. Marrack). Freshly isolated Ova-specific OTII T cells were obtained from lymph nodes from OTII transgenic mice[21]. T cells were brought into contact with dendritic cells by a quick centrifugation step at 600 *g*. at room temperature. Confocal microscopy analysis was performed immediately after 2 and 6 h.

Immunostaining of fixed dendritic cells

Five-day-old dendritic cells on coverslips were fixed in 3% paraformaldehyde in PBS, 1 mM Mg^{2+} and 0.1 mM Ca^{2+} (PBS-MC) for 10 min at 37 °C. Dendritic cells were washed extensively with PBS-MC and were permeabilized for 10 min with 0.5% saponin in PBS-MC at room temperature. Dendritic cells were washed and any excess of reactive groups of paraformaldehyde were quenched with 50 mM NH4Cl in PBS-MC for 15 min at room temperature. Anti-α tubulin (1:100, Oxford Biotechnology) staining was done in PBS-MC overnight at 4 °C. We used a rat anti-mouse Cy3-labelled secondary antibody for detection (Jackson Immunoresearch).

Received 4 April; accepted 3 July 2002; doi:10.1038/nature01004.

1. Villadangos, J. A. *et al.* Proteases involved in MHC class II antigen presentation. *Immunol. Rev.* **172,** 109–120 (1999).
2. Cosgrove, D. *et al.* Mice lacking MHC class II molecules. *Cell* **66,** 1051–1066 (1991).
3. Grusby, M. J., Johnson, R. S., Papaioannou, V. E. & Glimcher, L. H. Depletion of CD4 + T cells in major histocompatibility complex class II-deficient mice. *Science* **253,** 1417–1420 (1991).
4. Brown, M. S. & Goldstein, J. L. A receptor-mediated pathway for cholesterol homeostasis. *Science* **232,** 34–47 (1986).
5. Wubbolts, R. *et al.* Direct vesicular transport of MHC class II molecules from lysosomal structures to the cell surface. *J. Cell Biol.* **135,** 611–622 (1996).
6. Kleijmeer, M. *et al.* Reorganization of multivesicular bodies regulates MHC class II antigen presentation by dendritic cells. *J. Cell Biol.* **155,** 53–63 (2001).
7. Rowden, G. The Langerhans cell. *Crit. Rev. Immunol.* **3,** 95–180 (1981).
8. Maric, M. *et al.* Defective antigen processing in GILT-free mice. *Science* **294,** 1361–1365 (2001).
9. Hugo, P., Kappler, J. W., Godfrey, D. I. & Marrack, P. C. A cell line that can induce thymocyte positive selection. *Nature* **360,** 679–682 (1992).
10. Malissen, B., Steinmetz, M., McMillan, M., Pierres, M. & Hood, L. Expression of I-Ak class II genes in mouse L cells after DNA-mediated gene transfer. *Nature* **305,** 440–443 (1983).
11. Monks, C. R., Freiberg, B. A., Kupfer, H., Sciaky, N. & Kupfer, A. Three-dimensional segregation of supramolecular activation clusters in T cells. *Nature* **395,** 82–86 (1998).
12. Grakoui, A. *et al.* The immunological synapse: a molecular machine controlling T cell activation. *Science* **285,** 221–227 (1999).
13. Valitutti, S., Muller, S., Cella, M., Padovan, E. & Lanzavecchia, A. Serial triggering of many T-cell receptors by a few peptide-MHC complexes. *Nature* **375,** 148–151 (1995).
14. Underhill, D. M., Bassetti, M., Rudensky, A. & Aderem, A. Dynamic interactions of macrophages with T cells during antigen presentation. *J. Exp. Med.* **190,** 1909–1914 (1999).
15. Gunzer, M. *et al.* Antigen presentation in extracellular matrix: interactions of T cells with dendritic cells are dynamic, short lived, and sequential. *Immunity* **13,** 323–332 (2000).
16. Lanzavecchia, A. & Sallusto, F. Regulation of T cell immunity by dendritic cells. *Cell* **106,** 263–266 (2001).
17. Scholl, P. R. & Geha, R. S. MHC class II signalling in B-cell activation. *Immunol. Today* **15,** 418–422 (1994).
18. Mathis, D. J., Benoist, C., Williams, V. E., Kanter, M. & McDevitt, H. O. Several mechanisms can account for defective Eα gene expression in different mouse haplotypes. *Proc. Natl Acad. Sci. USA* **80,** 273–277 (1983).
19. Villadangos, J. A., Riese, R. J., Peters, C., Chapman, H. A. & Ploegh, H. L. Degradation of mouse invariant chain: roles of cathepsins S and D and the influence of major histocompatibility complex polymorphism. *J. Exp. Med.* **186,** 549–560 (1997).
20. Villadangos, J. A. *et al.* MHC class II expression is regulated in dendritic cells independently of invariant chain degradation. *Immunity* **14,** 739–749 (2001).
21. Barnden, M. J., Allison, J., Heath, W. R. & Carbone, F. R. Defective TCR expression in transgenic mice constructed using cDNA-based alpha- and beta-chain genes under the control of heterologous regulatory elements. *Immunol. Cell Biol.* **76,** 34–40 (1998).
22. Turley, S. J. *et al.* Transport of peptide-MHC class II complexes in developing dendritic cells. *Science* **288,** 522–527 (2000).

Supplementary Information accompanies the paper on *Nature*'s website (http://www.nature.com/nature).

Acknowledgements

We thank M. Boxem for help in designing the targeting construct and T. Schmidt for blastocyst microinjections. We thank A. W. M. van der Velden for providing DsRed1-labelled *S. typhimurium*, and we acknowledge discussions with members of the Ploegh laboratory.

Competing interests statement

The authors declare that they have no competing financial interests.

Correspondence and requests for materials should be addressed to H.L.P. (e-mail: ploegh@hms.harvard.edu).

Dendritic cell maturation triggers retrograde MHC class II transport from lysosomes to the plasma membrane

Amy Chow, Derek Toomre, Wendy Garrett & Ira Mellman

Department of Cell Biology and Section of Immunobiology, Ludwig Institute for Cancer Research, Yale University School of Medicine, 333 Cedar Street, PO Box 208002, New Haven, Connecticut 06520-8002, USA

Central to the initiation of immune responses is recognition of peptide antigen by T lymphocytes. The cell biology of dendritic cells makes them ideally suited for the essential process of antigen presentation[1]. Their life cycle includes several stages characterized by distinct functions and mechanisms of regulation[2]. Immature dendritic cells synthesize large amounts of major histocompatibility complex class II molecules (MHC II), but the αβ-dimers are targeted to late endosomes and lysosomes (often referred to as MHC class II compartments) where they reside unproductively with internalized antigens. After exposure to microbial products or inflammatory mediators, endocytosis is downregulated, the expression of co-stimulatory molecules is enhanced, and newly formed immunogenic MHC II–peptide complexes are transported to the cell surface[3–10]. That these MHC II molecules reach the surface is surprising, as the lysosomes comprise the terminal degradative compartment of the

endocytic pathway from which exogenous components generally cannot be recovered intact[11]. Here we have visualized this pathway in live dendritic cells by video microscopy, using cells expressing MHC II tagged with green fluorescent protein (GFP). We show that on stimulation, dendritic cells generate tubules from lysosomal compartments that go on to fuse directly with the plasma membrane.

Immunofluorescence microscopy of fixed cells shows that MHC class II–peptide complexes form in late endosomes and lysosomes on maturation of dendritic cells, and subsequently in a non-lysosomal compartment of class II vesicles and on the plasma membrane[8]. Electron microscope analysis of a dendritic-cell-like cell line further suggests activation correlated with the marked tubulation of lysosomal membranes[12]. The experiments reported here were undertaken to establish the kinetic relationship and functional significance of these events. GFP-tagged MHC II molecules were expressed in live bone-marrow-derived dendritic cells using a recombinant retrovirus. In the mouse, MHC II molecules are encoded by two loci, *I–A* and *I–E*. C57BL/6 mice have a mutation that abolishes production of the I–Eα chain[13]. The I–Eβ chain is produced normally, but in the absence of endogenous I–Eα it is retained in the endoplasmic reticulum (ER). We exploited this knockout and expressed a complementing I–Eα chain containing a cytoplasmic enhanced GFP tag (EGFP).

Dendritic cell cultures were infected on day 2 while the cells were still proliferating progenitors; expression was assayed on day 4 after differentiation into immature dendritic cells. Viral transduction was efficient, with about 50% of the CD11c-positive dendritic cells (32% of all cells) being GFP positive (Fig. 1a, left). To determine whether the I–Eα-GFP chain formed a dimer with endogenous I–Eβ, we stained the infected cell populations with an anti-MHC II antibody (14.4.4S) that recognizes only the paired I–Eαβ complex[14]. Properly assembled I–Eαβ dimers were found both by fluorescence-activated cell sorting (FACS) (Fig. 1a, right) and by immunofluorescence. As shown in Fig. 1b, the GFP signal co-localized with 14.4.4S predominantly in intracellular structures (see below). In contrast, infected MHC II-negative cells exhibited the unpaired GFP-tagged α-chain in an ER-like pattern (Fig. 1b). Moreover, about 50% of the

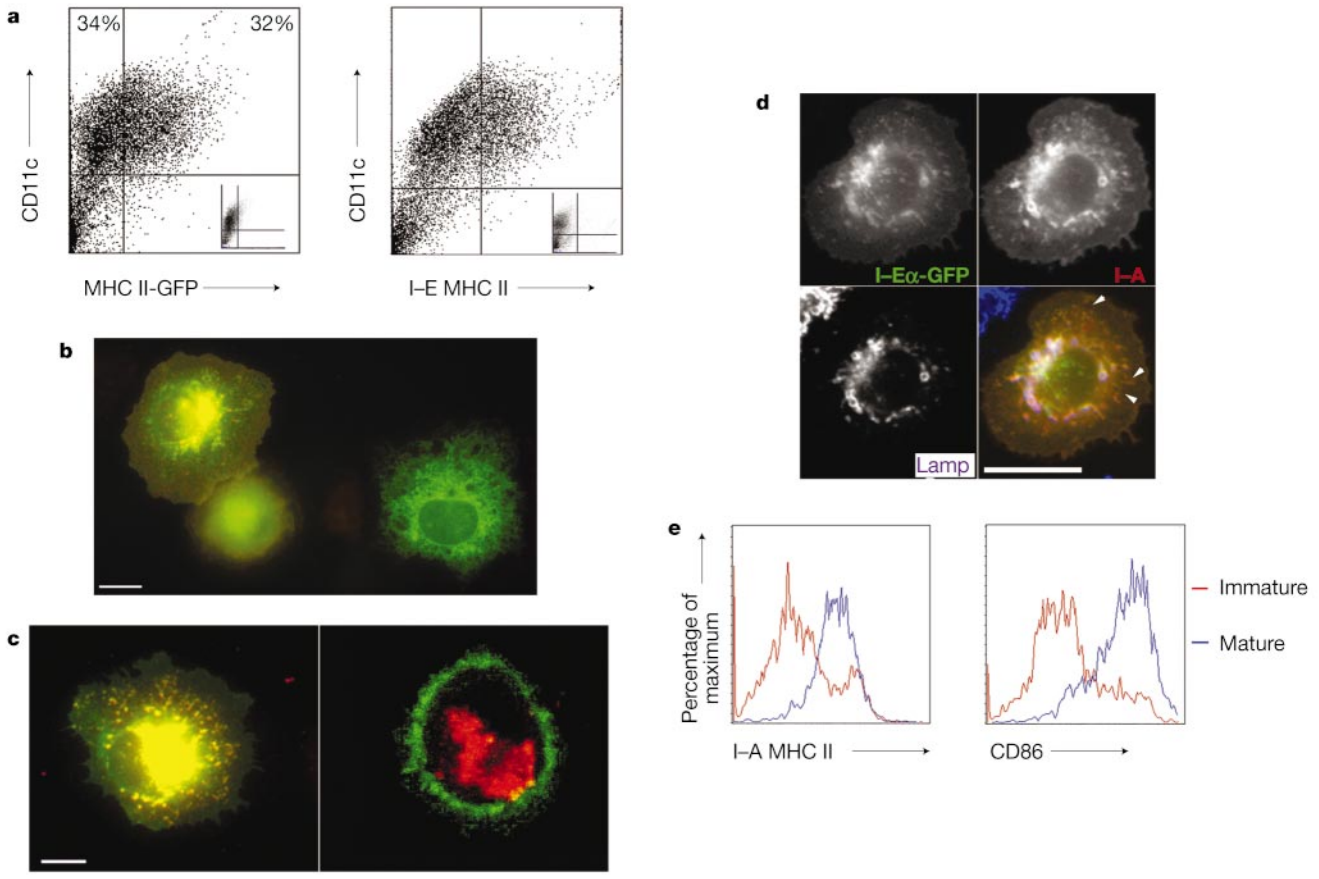

Figure 1 MHC II-GFP expressed by dendritic cells exhibit properties characteristic of endogenous MHC II. **a**, CD11c$^+$ dendritic cells express MHC II-GFP and localize I–Eαβ to the cell surface. Transduced dendritic cells were stained with cychrome-conjugated anti-CD11c alone (left) or together with phycoerythrin (PE)-conjugated 14.4.4S (which recognizes the I–Eαβ complex) (right), and analysed by flow cytometry. Total population percentages are indicated for upper quadrants (left). Insets show the same FACS profiles of untransduced dendritic cells. **b**, 14.4.4S-reactive I–Eαβ localizes intracellularly with MHC II-GFP. Optically merged fixed cell images show I–Eαβ complexes depicted in red and MHC II-GFP in green. I–Eαβ complexes co-localized with MHC II-GFP (yellow) in a dendritic cell, whereas a reticular ER-like pattern of MHC II-GFP was seen in a transduced cell negative for endogenous MHC II (not a dendritic cell). Scale bar, 10 μm. **c**, MHC II-GFP exhibited proper cellular localization in immature and mature dendritic cells. The left panel shows that MHC II-GFP accumulated predominantly in lysosomes in immature dendritic cells. The optically merged image shows an immature dendritic cell with Lamp-2 depicted in red and MHC II-GFP in green. Lamp-2 localizes together with MHC II-GFP (yellow). The right panel shows that live mature dendritic cells express high levels of MHC II-GFP on the cell surface with a clustered lysosomal distribution. The optically merged confocal image shows a mature dendritic cell with Texas red-dextran-loaded lysosomes in red and MHC II-GFP in green. Scale bar: 10 μm. **d**, MHC II-GFP localizes together with endogenous I–A MHC II in class II vesicles after stimulation. White arrowheads in the optically merged three-colour image indicate non-lysosomal compartments in which MHC II-GFP (green) and I–A (red) localize together. Scale bar, 10 μm. **e**, MHC II-GFP-expressing dendritic cells exhibit normal maturation markers. FACS histogram overlays show transduced dendritic cells labelled with PE-conjugated anti-I–A^b or PE-conjugated anti-CD86. Acquisitions were gated on MHC II-GFP$^+$ populations. Red line, immature dendritic cells; blue line, mature dendritic cells.

GFP-tagged MHC II molecules formed a dimer that was stable to SDS at room temperature (detected by western blot with an anti-GFP antibody), suggesting that the MHC II-GFP molecule was peptide loaded (not shown).

Although the I–Eα-EGFP chain formed αβ-dimers, it was essential to determine whether the tagged MHC II molecules exhibited the same intracellular distribution as their endogenous counterparts. As expected, in immature dendritic cells MHC II-GFP co-localized extensively with Lamp-2 (also known as lgp-B), a marker of the lysosomal membrane (Fig. 1c, left). Little MHC II-GFP was found at the cell surface. A markedly different distribution was found after treatment with lipopolysaccharide (LPS). In live mature dendritic cells, lysosomes were depleted of MHC II-GFP, most of which was now at the plasma membrane (Fig. 1c, right), as found previously in fixed cells[5,8]. Live confocal imaging revealed that surface MHC II-GFP was not re-internalized to lysosomes, but remained at the surface (See Supplementary Information 1C).

During maturation, dendritic cells exhibit a transient intermediate phenotype in which MHC II molecules are found in peripheral, non-lysosomal class II vesicles[7,11]. By immunofluorescence of dendritic cells fixed shortly after LPS stimulation, I–Eα-GFP could be found together with endogenous I–A molecules in Lamp-negative class II vesicles (Fig. 1d, arrows). In addition, FACS analysis revealed that after LPS stimulation, assembled I–E and I–A molecules appeared at the cell surface with similar kinetics (not shown). Thus, MHC II-GFP was fully functional and appeared to exhibit the same general pattern of intracellular transport as endogenous MHC II in immature and mature dendritic cells.

As a further control, we found that the retroviral expression system—or expression of the GFP-tagged construct—did not by itself interfere with or induce dendritic cell maturation. Although infected by defective virus, immature dendritic cells upregulated surface expression of endogenous I–A and CD86 normally in response to a maturation signal (Fig. 1e).

Having established that MHC II-GFP molecules form αβ-dimers that exhibit the expected intracellular distributions, we next asked whether the tagged MHC II molecules could exit from the lysosomes (MHC II compartments) of immature dendritic cells on maturation. Immature dendritic cells expressing MHC II-GFP were visualized by live-cell video confocal microscopy with or without addition of a maturation stimulus. MHC II-GFP-positive structures (presumably lysosomes) in unstimulated dendritic cells remained quiescent for up to 60 min, exhibiting limited saltatory movement in the perinuclear cytoplasm (Fig. 2a; see also Supplementary Information 2A). In contrast, less than 30 min after stimulation by LPS, the lysosomal structures exhibited marked movement and morphological changes, characterized especially by the formation of extensive tubules labelled with MHC II-GFP that extended 5–10 μm in length (Fig. 2b, left, red arrowheads; see also Supplementary Information 2B). Within 2 h, MHC II-GFP began to appear on the plasma membrane (right). At higher magnification and faster acquisition rates, the tubules were clearly transient structures, separating from their sites of origin and moving centrifugally towards the cell periphery (Fig. 2c; see also Supplementary Information 2C). The behaviour of an individual tubule, highlighted in the boxed area, is shown as individual frames (Fig. 2c, 0–20 s). The three-colour/three-time-point merged image (Fig. 2c) highlights the large degree of tubulation, extension and transport that

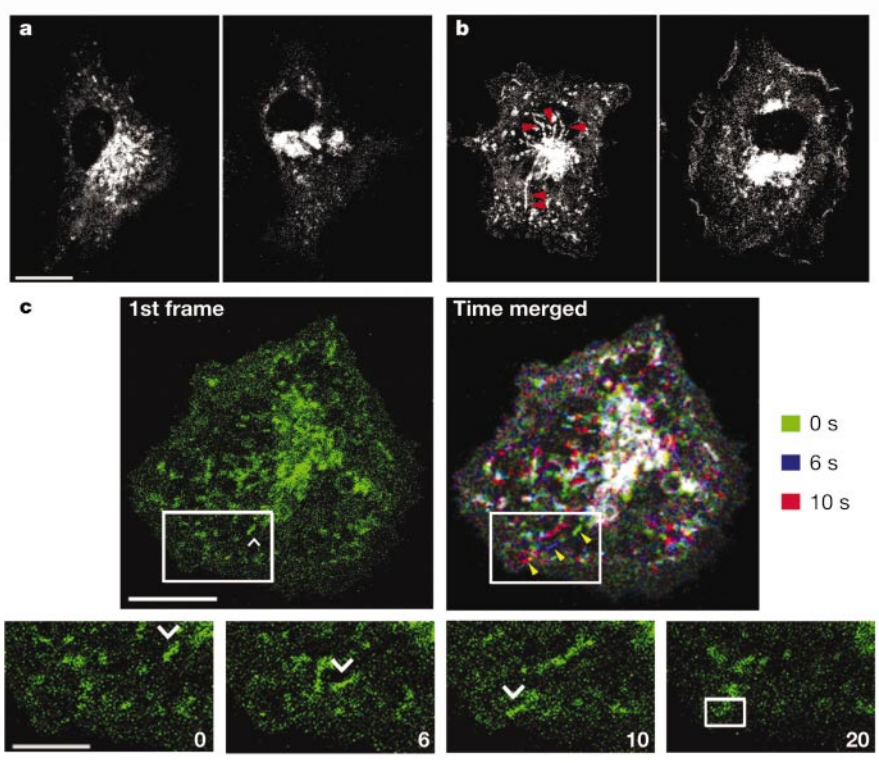

Figure 2 Export of MHC II-GFP molecules from lysosomes to the cell periphery occurs in tubular-vesicular structures in live dendritic cells imaged by confocal microscopy. **a**, Unstimulated dendritic cells remain quiescent from the start of live-cell imaging (left) until 4 h later (right). **b**, Stimulated dendritic cells form tubules within 30 min of stimulation (left, red arrowheads; a long tube is highlighted by a double arrowhead) and transport MHC II to the plasma membrane by 4 h (right). Scale bar, 10 μm. **c**, MHC II-GFP$^+$ tube-like structures in stimulated dendritic cells emanate from a perinuclear region, transit to the cell periphery, and disappear. The top left panel is an image of a cell corresponding to the first time frame, enlarged in individual frames below. Scale bar, 10 μm. The top right panel is a time overlay of a cell indicating directionality of MHC II-GFP transport. Structures that do not move over the 10-s period appear white. A tubule moving towards the cell periphery is marked with yellow arrowheads. The bottom panels are labelled with time frame intervals in seconds. A single translocating tubule is labelled with a white arrowhead and disappears at 20 s (white box). Scale bar, 5 μm.

occurred throughout the cell in just a single 10-s window. Of the 15 unstimulated dendritic cells that were examined, only two formed a limited number of short tubules, in contrast to the more than 50 stimulated cells analysed, all of which exhibited dynamic tubules.

Thus, most of the tubules emanated directly from late endosomes or lysosomes, as demonstrated by dual colour imaging of MHC II-GFP molecules in dendritic cells whose lysosomes had been loaded with Texas red-dextran (Fig. 3a). Formed over a time course of about 30 s, the GFP-labelled tubules were largely devoid of Texas red-dextran suggesting that nascent tubules excluded the bulk of lysosomal contents, presumably owing to their restricted internal volume. These data provide direct confirmation that the class II vesicles observed previously in fixed, maturing dendritic cells were, in fact, lysosome-derived elements[8].

We performed the same experiment except this time we used cells loaded with Cy3-labelled hen egg lysozyme (HEL), a model antigen that on dendritic-cell maturation contributes peptides that associate with MHC II in lysosomes[8]. As shown in low magnification (Fig. 3b, top; see also Supplementary Information 3B), numerous tubules (arrowheads) extend from the perinuclear area, which was intensely labelled for both MHC II-GFP (green) and Cy3-HEL (red; the large area of overlap is yellow). Many tubules were yellow, suggesting that they contained Cy3-HEL. To better illustrate this point, three consecutive video frames are shown, focusing on a single nascent tubule at higher magnification (Fig. 3b, bottom). The tubule clearly contains both markers. The reasons for the appearance of Cy3-HEL, but not Texas red-dextran, in the tubules are unclear. It may reflect the ability of HEL to associate with MHC II molecules or the propensity of this cationic protein to bind to the highly anionic lysosomal membrane. In either event, the presence of previously internalized Cy3-HEL in tubules confirmed their lysosomal origin and provided a convenient approach to identifying the origin of any tubule (see below).

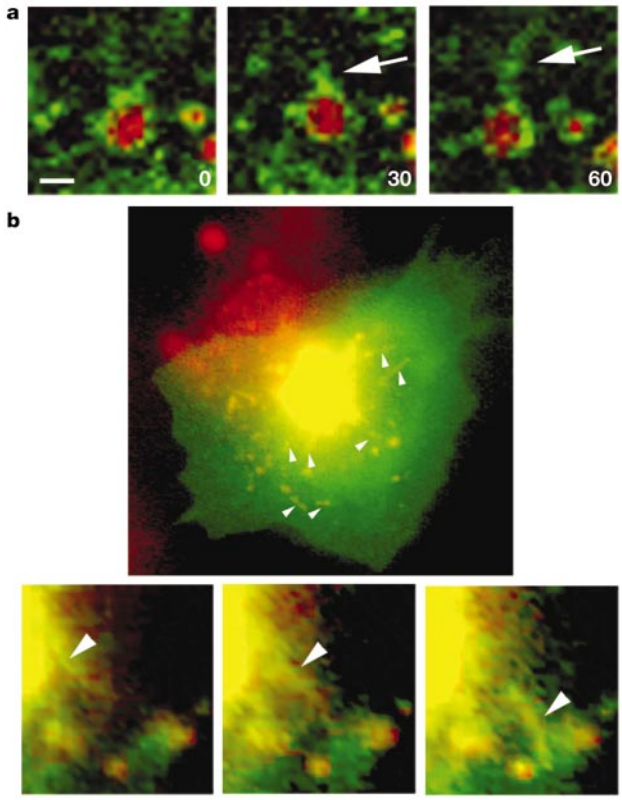

Figure 3 MHC II-GFP tubules originate from lysosomal/late endosomal compartments. **a**, MHC II-GFP$^+$ tubules (white arrows) extend from lysosomes loaded with Texas red-dextran over a time course of about 30 s. Panels are labelled with time frame intervals in seconds. Scale bar, 1 μm. **b**, Stimulated dendritic cells loaded with Cy3-HEL (red) extend several MHC II-GFP (green) tubules, which are also positive for Cy3-HEL and thus appear yellow (white arrowheads). An MHC II-negative cell that took up Cy3-HEL is in the background (upper left) positioned on top of the MHC II-GFP$^+$ dendritic cell. Three individual frames (1-s intervals) better illustrate a single double positive tubule (white arrowhead) extending from the perinuclear region.

Demonstrating that lysosomes can form dynamic and motile tubules after the onset of maturation does not in itself prove that these structures mediate the transfer of MHC II-GFP to the cell surface. To determine directly whether these tubules not only move to the periphery but actually fuse with the plasma membrane, we imaged MHC II-GFP transport in dendritic cells using combined epifluorescence (EPI) and total internal reflectance fluorescence microscopy (TIR-FM)[15]. TIR-FM (also known as evanescent wave microscopy) is one of the few techniques that allows a direct observation of fusion, and has been used to image exocytosis of secretory granules, Golgi-derived vesicles and even single synaptic vesicles[16–19]. In TIR-FM, a beam of light undergoes total internal reflection at the cell–coverslip interface. The light intensity decays exponentially away from the coverslip; hence only a very thin 'evanescent' layer (less than 200 nm) is illuminated at the bottom surface of a cell. We first compared TIR-FM images with EPI images collected from the same cell (Fig. 4a). In any single frame, MHC II-GFP molecules imaged by TIR-FM (left) yielded an entirely different pattern than when imaged by EPI (middle). As expected, TIR-FM of dendritic cells expressing MHC II-GFP revealed only those areas of the cell near the coverslip; note the lack of TIR fluorescence in the EPI region where the cell lifts off the coverslip. Bright spots in the TIR-FM image indicate tubular-vesicular structures closely associated or morphologically 'tethered' near the cell surface, some of which later fused. As expected, the EPI signal (green) was largely excluded from these regions and instead showed an accumulation of MHC II-GFP (red) in the perinuclear region (merged image, right).

To better illustrate the flux of fluorescence intensity during fusion, a single image of a stimulated dendritic cell was represented using a pseudo-colour scale (Fig. 4b, left; see also Supplementary Information 4B-1, B-2). Candidate fusions were seen all over the attached surface. In total, 25 cells were imaged in these experiments with over 200 fusion events detected (see Methods). One such event is shown over a 36-s time course (Fig. 4b, right). The vesicle/tubule approached the plasma membrane as seen by EPI. As the carriers approached the membrane they were also visible by TIR-FM. During fusion the TIR signal became momentarily brighter (22 s, red arrow) as the vesicle coalesced into the membrane, then dissipated as the membrane protein diffused into the plane of the membrane (23 s, blue arrow). Concomitant with the initial increase of the TIR signal at fusion, the EPI signal diminished, suggesting that fusion had occurred—if the vesicle had not fused and instead detached from the membrane surface, an EPI image would have remained. Although these images suggest a simple diffusive dissipation[15,19], closer analysis of the post-fusion diffusion kinetics may reveal maintenance of a preformed complex or cluster of MHC II molecules, as previously suggested on the basis of fixed images[8]. Using TIR-FM with an even shallower penetration depth should, in the future, allow us to investigate this matter more fully as it would substantially improve the signal-to-noise ratio. It is also possible that the clusters observed earlier are not derived from the fusion events but rather form after reaching the surface.

To monitor the origin of the tubules before their final fusion, we performed a combination of TIR-FM with two-colour EPI imaging. This approach allowed us to examine the behaviour of an MHC II-GFP-labelled tubule that could be identified definitively as having come from lysosomes owing to its Cy3-HEL content. Through the use of EPI, video imaging revealed abundant perinuclear lysosomes that were double positive for MHC II-GFP (red) and Cy3-HEL

(blue). In addition, many of the associated tubular elements appeared positive for both markers (Fig. 4c, boxed area and individual frames, yellow arrow). The fusion of a single, double positive Cy3-HEL and MHC II-GFP tubule was illustrated in a series of video frames that separately show the MHC II-GFP TIR-FM signal, the EPI signals for both MHC II-GFP and Cy3-HEL, and a merge of MHC II-GFP TIR-FM (green) and EPI (red) signals (Fig. 4c; 1–16 s; see also Supplementary Information 4C-1, C-2). In the first frame, a single tubule positive for both Cy3-HEL and MHC II-GFP is shown. With time, as the tubule approached the membrane, both EPI signals decreased while the MHC II-GFP TIR-FM signal increased (red arrow marks the maximum level). Fusion occurred by 15 s after which time the signal dissipated (blue arrow). Therefore, by using two-colour EPI combined with TIR-FM imaging we were able to track the formation, transport and ultimate plasma membrane fusion of MHC II-GFP-containing tubules derived from lysosomes.

Thus, dendritic cell lysosomes can initiate a previously unknown retrograde pathway by which selected components can be rescued from degradation and transferred to the plasma membrane. This tubule-mediated pathway is probably not unique to dendritic cells, but was identified here owing to its synchronous induction on dendritic cell maturation. On the other hand, the capacity for tubule formation may reflect a specialization of dendritic cell lysosomes. There is as yet scant evidence to indicate that MHC II-containing late endocytic compartments in dendritic cells or other antigen-presenting cells comprise a vesicle population physically distinct from conventional late endosomes and lysosomes[20,21]. The dendritic cell retrograde pathway is clearly distinct from exocytosis of 'secretory lysosomes' in natural killer cells or cytotoxic T lymphocytes[22], lysosomes expressing MHC II-GFP in MelJuSo cells[23], or multivesicular bodies (exosomes) in B cells[24]. These processes are morphologically distinct and also result in the release of bulk lysosomal contents. Although lysosomes are well known to form tubular extensions in macrophages and B cells in response to certain activators[25,26], these tubules do not mediate transport to the cell surface but instead may facilitate phagosome–lysosome fusion. The mechanisms that induce tubule formation are unclear. Extension

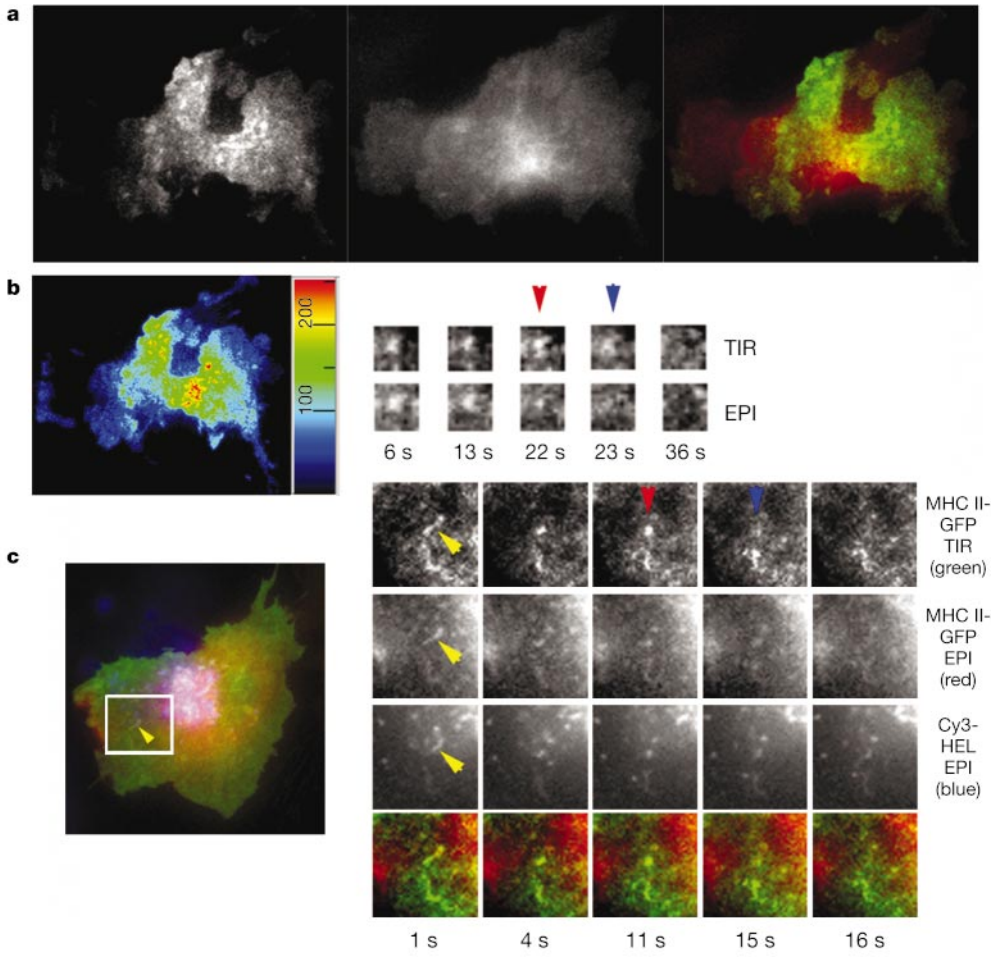

Figure 4 Combined TIR-FM/EPI microscopy demonstrates fusion of lysosome-derived MHC II-GFP structures with the plasma membrane. **a**, TIR-FM (left) illuminates only the cell surface at sites close to the coverslip, whereas EPI (middle) illuminates the entire cell. A merged image (right) highlights differences between the two types of illumination (see text). **b**, Fusion of MHC II-GFP with plasma membrane, indicated by a flash of fluorescence followed by a dissipating signal. The left panel shows a single TIR image represented by a pseudo-colour scale (red, highest fluorescence intensity; blue, lowest fluorescence intensity). Red spots reflect sites of intense membrane activity and candidate fusion events. Supplementary Information 4B illustrates the large number of events that occur. The right panels show sequential frames of a single fusion event simultaneously imaged by TIR-FM and EPI. Note that the fluorescence signal disappears in the corresponding EPI images (bottom row). **c**, One-colour TIR-FM and two-colour EPI imaging of an MHC II^+ tubule fusing with the plasma membrane: green, TIR; red, EPI of MHC II-GFP; blue, EPI of Cy3-HEL. The left panel shows a three-colour merge of the first frame highlighting a single tubule that is positive in all three imaging modes. This tubule is enlarged in colour-separated panels showing a 16-s sequence (right). The yellow arrowhead highlights the tubule present in all three channels. The TIR signal was highest at 11 s (red arrowhead) and dissipates at 15 s (blue arrowhead), suggesting a partial fusion event, as the Cy3-HEL signal at 15–16 s does not disappear entirely. The bottom row depicts a merge of MHC II-GFP TIR-FM and MHC II-GFP EPI channels (see Supplementary Information 4C).

along microtubules is probable as is the case for other tubulation events[27]; however, microtubule disruption does not block the recruitment of MHC II from lysosomes[8]. Also unknown is the degree to which retrograde transport involves selective sorting between MHC II and resident lysosomal membrane components. These and other issues can now be addressed easily using various combinations of recombinant retroviruses together with live cell imaging. □

Methods

Cell culture

Dendritic cells were generated from mouse bone marrow as described previously[28]. In brief, bone marrow cells from C57BL/6 mice (Jackson Laboratories) were depleted of erythrocytes, T cells, B cells, granulocytes and MHC II-positive cells and subsequently cultured in RPMI (GIBCO) supplemented with 5% FCS, recombinant mouse granulocyte/macrophage-colony stimulating factor (GM-CSF), 20 $\mu g\,ml^{-1}$ gentamycin and 50 μM β-mercaptoethanol (dendritic cell growth media). Recombinant mouse GM-CSF was produced as culture supernatant from J558L cells transfected with the mouse GM-CSF (a gift of D. Gray). Before dendritic cell differentiation, proliferating precursors were infected with retrovirus on day 2 of culture as described previously[29]. Non-adherent cells were removed carefully and fresh media was added every two days. Immature dendritic cells were imaged on days 4 and 5 of culture. Mature dendritic cells were generated by adding 100 $ng\,ml^{-1}$ LPS (Sigma) or bacteria to disaggregated and replated cultures for 24–48 h.

Antibodies

For FACS, staining was performed using the following antibodies: PE-conjugated 14.4.4S, PE-conjugated CD86, PE-conjugated anti-I–A^b and cychrome-conjugated anti-CD11c (all from Pharmingen). Mouse I–Eαβ dimers were detected by 14.4.4S, a mouse anti-mouse monoclonal antibody, and mouse Lamp-2 using the rat anti-mouse monoclonal antibody[5]. Alexa 594-conjugated goat anti-mouse or goat anti-rat secondary antibodies (Molecular Probes) were used for detection.

Retrovirus generation and transduction

Retrovirus was generated in ΦNX-ecotropic cells as previously described[30]. I–Eα-GFP was constructed by polymerase chain reaction (PCR)-based mutagenesis (based on Stratagene QuikChange technique), creating a Bgl site at the 3′ end of IEα (using the oligonucleotide 5′-CGACAAGGAGCCCTGAGATCTACCTGGAGGTGCGTTAAATGTGC and 3′-GCACATTTAACGCACCTCCAGGTAGATCTCAGGGCTCCTTGTCG) and eliminating the stop codon. EGFP (a gift from T. Hughes) was fused in-frame using the Bgl site. The resulting fusion construct I–Eα-EGFP was cloned into LZRS-pBMN using *EcoR*I sites. This viral vector was transfected into ΦNX-ecotropic cells using Fugene (Roche). We obtained stable transfectants after selection in puromycin. Virus was collected in dendritic cell growth medium for 24 h and used to infect dendritic cells. Infection was performed by adapting a previously described method[29]. Briefly, virus was collected and supplemented with polybrene (8 $\mu g\,ml^{-1}$) and HEPES (10 mM) and added to dendritic cell cultures. Tissue culture plates were spun in a table-top centrifuge at 32 °C, 2,500 r.p.m. (1,200*g*) for 2 h. Virus was removed and fresh medium was added. Expression was assayed 48 h after infection.

Confocal microscopy

To label lysosomes, day 4–5 immature dendritic cells were loaded with Texas red-dextran (Molecular Probes) at a concentration of 250 $\mu g\,ml^{-1}$ for 30 min, chased with fresh medium for 30 min and plated for 30 min on poly-L-lysine pre-coated number 1.5 coverslips attached to 35-mm dishes (MatTek). Fresh dendritic cell growth medium supplemented with 10 mM HEPES (Gibco) was added to the plate along with LPS or bacteria if the cells were to be stimulated. Cells were imaged on a Zeiss LSM 510 confocal microscope equipped with a × 100 1.4 NA Plan-Apochromat oil-immersion lens. The cell chamber was heated to 37 °C using a Tempcontrol Digital 37-2 device (Warner Instruments). Laser lines at 488 nm and 545 nm were used for excitation of GFP and Texas red, and emissions wavelengths were separated by band pass (505–530 nm) and long pass (585 nm) filters, respectively. To minimize photobleaching, laser power was typically under 2% of maximum and the pinhole size was set to 1.0–1.2. Framescan rates varied from 1.9 to 3.9 s with a line average of 2; multi-tracking (line switching) was used for two-colour imaging. Acquisition was performed using Zeiss LSM 510 version 3.0 software and processing was completed using Adobe Photoshop 5.5 and Openlab 3.0 (Improvision). Movies were assembled using Graphic Converter version 3.8.

TIR-FM and analysis

TIR-FM was achieved using an objective-type set-up. An Olympus IX-70 inverted microscope was fitted with an Olympus × 60 1.45 NA Plan-apochromat TIR-FM oil-immersion lens, mounted on a piezo-electric focus drive (Physics Instruments). Cells were plated on MatTek coverslip dishes as above, and were imaged at 32–35 °C in a heated room. For TIR illumination a 488-nm, 100 mW argon laser (Melles Griot) was electronically shuttered and coupled via single mode fibre (KineFLEX; PointSource) to a dual fibre TIR/monochromator condenser (Till Photonics). TIR illumination used in this configuration had an estimated penetration depth ($1/e$) of about 93 nm, assuming refractive index $n_{cytosol} \approx 1.36$ and TIR critical angle $\theta_{max} \approx 69.7°$ (for calculation see ref. 15). For epi-illumination, we used an electrically shuttered Polychrome IV monochromator (Till Photonics). Light passed through a dual GFP/dsRed TIR filter block (AHF Analysentechnik) and was detected with an Imago QE-cooled charge-coupled device (CCD) camera (PCO; full chip, 1,376 × 1,040 pixel, 6.45 μm^2 per pixel, 16 MHz scan rate). Rapid sequential (less than 10-ms delay) TIR and EPI illumination was accomplished using Till Photonics hardware controller and TillVision software. Typically, dual images were acquired at 1–2 Hz with 2 × 2 binning and exposure times of 400 ms and under 50 ms for TIR and EPI illumination, respectively. Post acquisition analysis and processing were done using macros in TillVision software. For analysis of individual fusion events, a 5 × 5 pixel square was centred around the fusion site and the average pixel intensity was measured over time. Fusion events were specifically identified by a 'signature' fusion intensity profile[15] and correlated with loss of signal in both the EPI and TIR channels. By these criterion a fusing vesicle gave a different signal than a fluorescent patch or a vesicle that approaches the cell surface and subsequently retreats into the cell. Note, however, at the current penetration depth of about 100 nm, fusion events are still relatively dim. Fusion events were manually detected and counted while looping 300–6,000 time-lapse frames. Images were exported as TIFF images, processed using Adobe Photoshop version 5.5 and converted into QuickTime movies using Graphic Converter version 3.8.

Received 22 April; accepted 2 July 2002; doi:10.1038/nature01006.

1. Banchereau, J. & Steinman, R. M. Dendritic cells and the control of immunity. *Nature* **392,** 245–252 (1998).
2. Mellman, I. & Steinman, R. M. Dendritic cells: specialized and regulated antigen processing machines. *Cell* **106,** 255–258 (2001).
3. Cella, M., Engering, A., Pinet, V., Pieters, J. & Lanzavecchia, A. Inflammatory stimuli induce accumulation of MHC class II complexes on dendritic cells. *Nature* **388,** 782–787 (1997).
4. Garrett, W. S. *et al.* Developmental control of endocytosis in dendritic cells by Cdc42. *Cell* **102,** 325–334 (2000).
5. Pierre, P. *et al.* Developmental regulation of MHC class II transport in mouse dendritic cells. *Nature* **388,** 787–792 (1997).
6. Pierre, P. & Mellman, I. Developmental regulation of invariant chain proteolysis controls MHC class II trafficking in mouse dendritic cells. *Cell* **93,** 1135–1145 (1998).
7. Inaba, K. *et al.* The formation of immunogenic major histocompatibility complex class II-peptide ligands in lysosomal compartments of dendritic cells is regulated by inflammatory stimuli. *J. Exp. Med.* **191,** 927–936 (2000).
8. Turley, S. J. *et al.* Transport of peptide-MHC class II complexes in developing dendritic cells. *Science* **288,** 522–527 (2000).
9. Sallusto, F., Cella, M., Danieli, C. & Lanzavecchia, A. Dendritic cells use macropinocytosis and the mannose receptor to concentrate macromolecules in the major histocompatibility complex class II compartment: downregulation by cytokines and bacterial products. *J. Exp. Med.* **182,** 389–400 (1995).
10. West, M. A., Prescott, A. R., Eskelinen, E. L., Ridley, A. J. & Watts, C. Rac is required for constitutive macropinocytosis by dendritic cells but does not control its downregulation. *Curr. Biol.* **10,** 839–848 (2000).
11. Kornfeld, S. & Mellman, I. The biogenesis of lysosomes. *Annu. Rev. Cell Biol.* **5,** 483–525 (1989).
12. Kleijmeer, M. *et al.* Reorganization of multivesicular bodies regulates MHC class II antigen presentation by dendritic cells. *J. Cell Biol.* **155,** 53–63 (2001).
13. Mathis, D. J., Benoist, C., Williams, V. E., Kanter, M. & McDevitt, H. O. Several mechanisms can account for defective Eα gene expression in different mouse haplotypes. *Proc. Natl Acad. Sci. USA* **80,** 273–277 (1983).
14. Ozato, K., Mayer, N. & Sachs, D. H. Hybridoma cell lines secreting monoclonal antibodies to mouse H-2 and Ia antigens. *J. Immunol.* **124,** 533–540 (1980).
15. Toomre, D., Steyer, J. A., Keller, P., Almers, W. & Simons, K. Fusion of constitutive membrane traffic with the cell surface observed by evanescent wave microscopy. *J. Cell Biol.* **149,** 33–40 (2000).
16. Steyer, J. A. & Almers, W. A real-time view of life within 100 nm of the plasma membrane. *Nature Rev. Mol. Cell Biol.* **2,** 268–275 (2001).
17. Toomre, D. & Manstein, D. J. Lighting up the cell surface with evanescent wave microscopy. *Trends Cell Biol.* **11,** 298–303 (2001).
18. Zenisek, D., Steyer, J. A. & Almers, W. Transport, capture and exocytosis of single synaptic vesicles at active zones. *Nature* **406,** 849–854 (2000).
19. Schmoranzer, J., Goulian, M., Axelrod, D. & Simon, S. M. Imaging constitutive exocytosis with total internal reflection fluorescence microscopy. *J. Cell Biol.* **149,** 23–32 (2000).
20. Pierre, P. *et al.* HLA-DM is localized to conventional and unconventional MHC class II-containing endocytic compartments. *Immunity* **4,** 229–239 (1996).
21. Kleijmeer, M. J., Morkowski, S., Griffith, J. M., Rudensky, A. Y. & Geuze, H. J. Major histocompatibility complex class II compartments in human and mouse B lymphoblasts represent conventional endocytic compartments. *J. Cell Biol.* **139,** 639–649 (1997).
22. Stinchcombe, J. C. & Griffiths, G. M. Regulated secretion from hemopoietic cells. *J. Cell Biol.* **147,** 1–6 (1999).
23. Wubbolts, R. *et al.* Direct vesicular transport of MHC class II molecules from lysosomal structures to the cell surface. *J. Cell Biol.* **135,** 611–622 (1996).
24. Raposo, G. *et al.* B lymphocytes secrete antigen-presenting vesicles. *J. Exp. Med.* **183,** 1161–1172 (1996).
25. Lankar, D. *et al.* Dynamics of major histocompatibility complex class II compartments during B cell receptor-mediated cell activation. *J. Exp. Med.* **195,** 461–472 (2002).
26. Racoosin, E. L. & Swanson, J. A. Macropinosome maturation and fusion with tubular lysosomes in macrophages. *J. Cell Biol.* **121,** 1011–1020 (1993).
27. Cole, N. B. & Lippincott-Schwartz, J. Organization of organelles and membrane traffic by microtubules. *Curr. Opin. Cell Biol.* **7,** 55–64 (1995).
28. Inaba, K. *et al.* Generation of large numbers of dendritic cells from mouse bone marrow cultures supplemented with granulocyte/macrophage colony-stimulating factor. *J. Exp. Med.* **176,** 1693–1702 (1992).
29. De Veerman, M. *et al.* Retrovirally transduced bone marrow-derived dendritic cells require $CD4^+$ T cell help to elicit protective and therapeutic antitumor immunity. *J. Immunol.* **162,** 144–151 (1999).
30. Kinsella, T. M. & Nolan, G. P. Episomal vectors rapidly and stably produce high-titer recombinant retrovirus. *Hum. Gene Therapy* **7,** 1405–1413 (1996).

Supplementary Information accompanies the paper on *Nature*'s website (http://www.nature.com/nature).

Acknowledgements

We thank members of the Mellman/Warren laboratory for general support and advice, in particular J. Seemann and L. Pelletier. We also thank J. Kagan, A. Neild and C. Roy for confocal microscopy assistance, L. Zheng and A. Bothwell for help with the retroviral system, and T. Hughes for providing the EGFP complementary DNA. We thank O. Bloom, J. Unternaehrer and J. Chow for critical reading of the manuscript, and Olympus for providing the TIR-FM microscope. We also thank the Ludwig Institute for Cancer Research and the NIH for their support of our work.

Competing interests statement

The authors declare that they have no competing financial interests.

Correspondence and requests for materials should be addressed to I.M. (e-mail: ira.mellman@yale.edu).

A chromatin remodelling complex that loads cohesin onto human chromosomes

Mohamed-Ali Hakimi*, Daniel A. Bochar*, John A. Schmiesing†, Yuanshu Dong*, Orr G. Barak*, David W. Speicher*, Kyoko Yokomori† & Ramin Shiekhattar*

** The Wistar Institute, 3601 Spruce Street, Philadelphia, Pennsylvania 19104, USA*

† University of California, Irvine, Department of Biological Chemistry, 240D, Med Sci I, Irvine, California 92697-1700, USA

Nucleosomal DNA is arranged in a higher-order structure that presents a barrier to most cellular processes involving protein DNA interactions[1]. The cellular machinery involved in sister chromatid cohesion, the cohesin complex, also requires access to the nucleosomal DNA to perform its function in chromosome segregation[2–10]. The machineries that provide this accessibility are termed chromatin remodelling factors[11]. Here, we report the isolation of a human ISWI (SNF2h)-containing chromatin remodelling complex that encompasses components of the cohesin and NuRD complexes. We show that the hRAD21 subunit of the cohesin complex directly interacts with the ATPase subunit SNF2h. Mapping of hRAD21, SNF2h and Mi2 binding sites by chromatin immunoprecipitation experiments reveals the specific association of these three proteins with human DNA elements containing Alu sequences. We find a correlation between modification of histone tails and association of the SNF2h/cohesin complex with chromatin. Moreover, we show that the association of the cohesin complex with chromatin can be regulated by the state of DNA methylation. Finally, we present evidence pointing to a role for the ATPase activity of SNF2h in the loading of hRAD21 on chromatin.

We have previously shown that human SNF2h resides in two distinct complexes in HeLa nuclear extract. These are a complex of relative molecular mass (M_r) 670,000 (670K), WCRF/hACF, that eluted in the 1 M KCl fraction of the phosphocellulose (P11) chromatography, and a larger complex of M_r 1,500–2,000K eluting in the 0.5-M KCl fraction of P11 (ref. 12). Moreover, immunoprecipitation of SNF2h from the 0.5-M or 1-M KCl eluate of P11 demonstrated the specific association of WCRF180/hACF1 only with the SNF2h in the 1-M P11 fraction (Fig. 1a). To determine the components of the larger SNF2h-containing complex found in the 0.5-M P11 fraction, we purified SNF2h following the scheme in Fig. 1b. Silver stain analysis of the last chromatographic step revealed the association of SNF2h with a complex of approximately 15 polypeptides (Fig. 1c). Western blot analysis of the Superose 6 column fractions indicated that SNF2h eluted with a broad profile encompassing the relative molecular masses of 2,000K to 670K (Fig. 1c). Interestingly, although the two-subunit WCRF/hACF complex could not be detected in the initial steps of the purification, the 670 K SNF2h-containing complex was shown eluting in fractions (33–36) of Superose 6 (Fig. 1c, see the western blot for WCRF180). A combination of ion trap mass spectrometry and western blot analysis identified the other components of the M_r 2,000K complex as subunits of the NuRD chromatin remodelling complex[13–15], and the polypeptides involved in the sister chromatin cohesion. All four subunits of the core-cohesin complex—SMC1, SMC3, SA1/SA2 and hRAD21—were identified by mass spectrometry. Western blot analysis confirmed the coelution of hRAD21 and components of the NuRD complex with SNF2h in fractions 27–30 (Fig. 1c). These findings indicate that a fraction of SNF2h displays a chromatographic profile consistent with being a component of a complex that also contains cohesin and the subunits of the NuRD complex.

To rigorously demonstrate that the cohesin-containing SNF2h

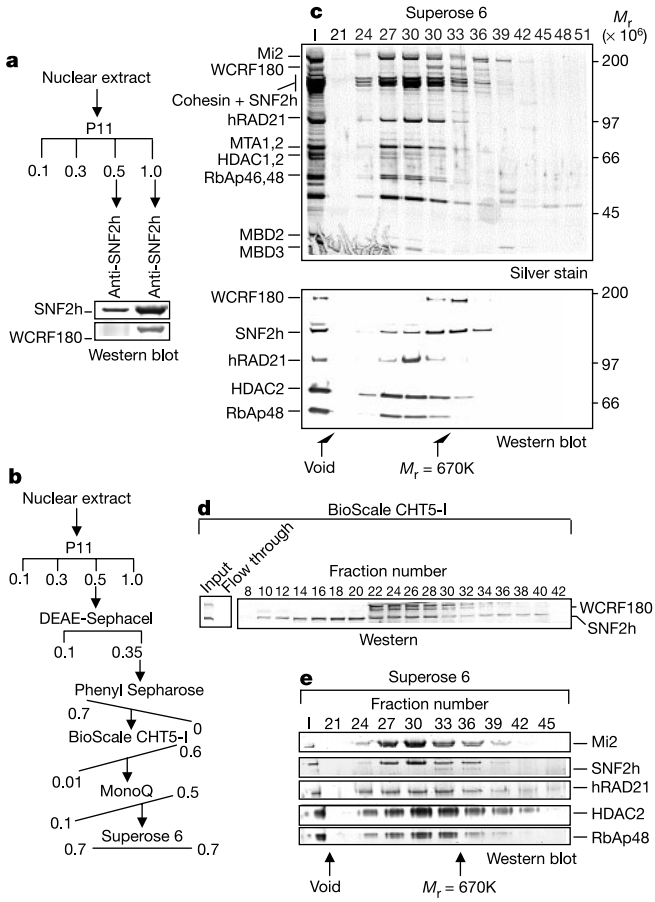

Figure 1 Isolation of an SNF2h complex containing cohesin. **a**, HeLa nuclear extract was fractionated by chromatography and the fractions shown by an arrow were used for affinity-purification followed by western blotting as described[24]. **b**, Purification scheme. HeLa nuclear extract was fractionated by chromatography as described in Methods. **c**, Silver staining and western blot analysis of Superose 6 fractions (15 μl). The proteins analysed are indicated to the left of the figure. **d**, Western blot analysis of BioScale CHT5-I column fractions using antibodies shown on the right of the figure. Fractions 18–20 were pooled for analysis on a subsequent Mono Q column. **e**, Western blot analysis of Superose 6 column fractions using antibodies against proteins to the right of the figure. Throughout this purification fractions containing WCRF were excluded.

